Int. J. Multiphase Flow Vol. 16, No. 1, pp. 139–151, 1990
Printed in Great Britain.

0301-9322/90 $3.00 + 0.00

TRANSIENT RESPONSE CHARACTERISTICS OF TWO-PHASE CONDENSING FLOWS

N. S. LIAO and C. C. WANG
Department of Mechanical Engineering, National Chiao Tung University, Taiwan, R.O.C.

(*Received* 16 *November* 1988; *in revised form* 6 *June* 1989)

Abstract—A theoretical and experimental investigation has been carried out into the transient response characteristics of the two-phase condensing flow in a double-pipe condenser. A two-phase two-fluid model, together with the constitutive relations, describes the dynamic behavior of the condensing flow. A semi-implicit finite difference scheme has been employed to solve the governing equations. The flow surge response in the condensate outlet flow to changes in (1) inlet pressure, (2) inlet vapor flow and (3) coolant flowrate are analyzed. The results are presented to show that the transient response of the condensing flow is very sensitive to changes in the condensing pressure. The response to change in the coolant side is relatively slow, due to the thermal capacity of the tube wall. Experimental data are presented which reveal the oscillatory characteristics of the resulting condensing flow transient due to changes in the coolant flowrate. This phenomenon has been well-interpreted by the present analysis.

Key Words: transient response, condensing flow, numerical modeling

1. INTRODUCTION

The dynamic characteristics of transient two-phase condensing flows are of interest to designers of industrial heat-removal systems associated with power generation, vapor compression refrigeration and chemical processing. In the literature, various types of dynamic characteristics due to system input changes have been reported for condensing flows. Schoenberg (1966) analyzed the responses of the condensing pressure and interface movement to sinusoidal variation in inlet vapor flow. His work was in connection with specific space power applications involving the condensation of mercury vapor inside a tube. McMorran & Moeck (1976), based on a drift–flux model, studied the frequency response of the condensing side of a reboiler associated with a heavy-water nuclear power plant. Wedekind & Bhatt (1977) reported experimental data which show that in condensing flow a small change in the inlet vapor flow would momentarily cause a very large flow surge in the outlet liquid flow. The results were predicted with a "system mean void fraction model" which they developed. Liao *et al.* (1988) analyzed the responses of void fraction and flowrate to changes in wall heat flux and inlet vapor flowrate, using a "void propagation equation" derived by Zuber & Staub (1966).

In all the above cited analyses, the momentum equations have not been included; important mechanisms associated with the transient condensing flow may thus have been lost. In this work, we employ a two-phase two-fluid model to analyze the transient phenomena in a double-pipe condenser. The effects of flow inertia, pressure variation, vapor compressibility and coolant flow conditions are all involved to highlight the essential mechanisms behind the transient phenomena of the condensing flow. An experimental study using freon-22 as the working fluid has been conducted to appraise the accuracy of the analytical results.

2. THEORETICAL FORMULATION

2.1. Field Equations

The physical model and its coordinate system are illustrated in figure 1. It is a condenser of double-pipe configuration, as shown. Refrigerant vapor flows in the inner tube while coolant flows in the annulus. The outer surface is insulated. Inside the tube, the flow geometry of the condensing flow is assumed annular with a liquid film around the periphery of the tube and a continuous gas flow in the core. The vapor and liquid phases have differing velocities which are assumed to be

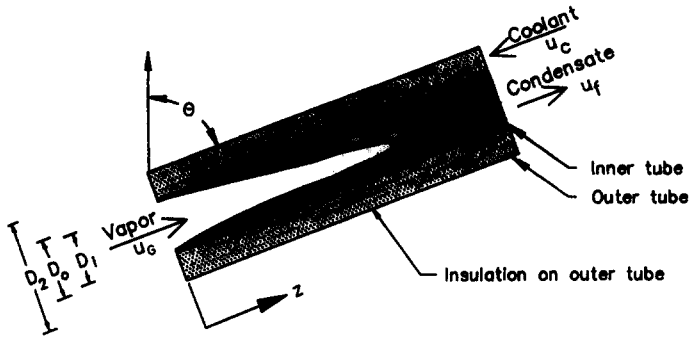

Figure 1. Physical configuration and coordinate system.

one-dimensional. In the condensing region, thermodynamic equilibrium between the phases is assumed to exist at any instant in time. The governing equations for this system are written as follows:

vapor mass equation,

$$\frac{\partial}{\partial t}(\epsilon\rho_G) + \frac{\partial}{\partial z}(\epsilon\rho_G u_G) = -\dot{\Gamma}; \quad [1]$$

liquid mass equation,

$$\frac{\partial}{\partial t}[(1-\epsilon)\rho_L] + \frac{\partial}{\partial z}[(1-\epsilon)\rho_L u_L] = \dot{\Gamma}; \quad [2]$$

vapor momentum equation,

$$\rho_G\epsilon\left(\frac{\partial u_G}{\partial t} + u_G\frac{\partial u_G}{\partial z}\right) = -\epsilon\frac{\partial p}{\partial z} - \rho_G g\epsilon\cdot\sin\theta - \frac{4\sqrt{\epsilon}}{D_i}\tau_i - F_v + \dot{\Gamma}(u_G - u_i); \quad [3]$$

and

liquid moment equation,

$$(1-\epsilon)\rho_L\left(\frac{\partial u_L}{\partial t} + u_L\frac{\partial u_L}{\partial z}\right) = -(1-\epsilon)\frac{\partial p}{\partial z} - \rho_L g(1-\epsilon)\cdot\sin\theta + \frac{4\sqrt{\epsilon}}{D_i}\tau_i + F_v - \frac{4}{D_i}\tau_w + \dot{\Gamma}(u_i - u_L). \quad [4]$$

Variables in the above equations have the following meanings:

D_i — inner diameter of the condenser tube;
g — acceleration due to gravity;
p — static pressure;
u_i — interfacial velocity;
u_G, u_L — gas and liquid velocities;
ϵ — void fraction;
θ — angle of condenser inclination from the vertical;
τ_i — interfacial shear stress;
τ_w — wall shear stress;
ρ_G, ρ_L — gas and liquid densities;

and

$\dot{\Gamma}$ — volumetric rate of condensation.

F_v in [3] and [4] represents the virtual mass force. It is known that the typical two-fluid model of two-phase flow possesses complex characteristics, and constitutes an ill-posed initial value problem. Lahey *et al.* (1980) pointed out that the inclusion of the virtual mass force helps to overcome these difficulties and improve the numerical efficiency. The general form of the virtual mass force, as

derived by Drew *et al.* (1979), is expressed by

$$F_v = \epsilon\rho_L C_v\left\{\frac{\partial u_G}{\partial t} - \frac{\partial u_L}{\partial t} + u_G\frac{\partial(u_G - u_L)}{\partial z} + (u_G - u_L)\left[(\lambda - 2)\frac{\partial u_G}{\partial z} + (1-\lambda)\frac{\partial u_L}{\partial z}\right]\right\}, \quad [5]$$

where C_v is the coefficient of virtual mass and λ is a constant. No & Kazimi (1985) have derived the quantitative bounds on λ and C_v from considerations of the second law of thermodynamics and numerical stability.

The last terms in [3] and [4] represent the momentum exchanges due to mass transfer between the phases. In these terms u_i is usually assumed to be equal to u_L (Yadigaroglu & Lahey 1976). In fact, a preliminary calculation has shown that choosing between u_G and u_L has little effect on the calculated results. Thus, $u_i = u_L$ is used in the present analysis.

For easier handling of the pressure terms, [3] and [4], with [5] substituted for F_v, are rearranged to become

$$\rho_G\epsilon\left(\frac{\partial u_G}{\partial t} + u_G\frac{\partial u_G}{\partial z}\right) + (1-\epsilon)\rho_L\left(\frac{\partial u_L}{\partial t} + u_L\frac{\partial u_L}{\partial z}\right) = -\frac{\partial p}{\partial z} - [\rho_G\epsilon + (1-\epsilon)\rho_L]\boldsymbol{g}\cdot\sin\theta - \frac{4}{D_i}\tau_w + \dot{\Gamma}(u_G - u_L) \quad [6]$$

and

$$\begin{aligned}&\epsilon[(1-\epsilon)\rho_G + \rho_L C_v]\frac{\partial u_G}{\partial t} - \epsilon[(1-\epsilon)\rho_L + \rho_L C_v]\frac{\partial u_L}{\partial t}\\ &\quad + \{[\epsilon(1-\epsilon)\rho_G + \epsilon\rho_L C_v(\lambda - 1)]u_G - \epsilon\rho_L C_v(\lambda - 2)u_L\}\frac{\partial u_G}{\partial z}\\ &\quad - \{[\epsilon(1-\epsilon)\rho_L + \epsilon\rho_L C_v(1-\lambda)]u_L + \epsilon\rho_L C_v\lambda u_G\}\frac{\partial u_L}{\partial z}\\ &= \dot{\Gamma}(1-\epsilon)(u_G - u_L) + \epsilon(1-\epsilon)(\rho_L - \rho_G)\boldsymbol{g}\cdot\sin\theta - \frac{4\sqrt{\epsilon}}{D_i}\tau_i - \frac{4\epsilon}{D_i}\tau_w. \end{aligned} \quad [7]$$

In the analysis of condensation in a double-pipe condenser, the equations governing the temperature variations in the tube wall and coolant flow are also involved. Assuming one-dimension, the wall conduction equation and the coolant energy equation, respectively, are

$$\tfrac{1}{4}(D_o^2 - D_i^2)\rho_w c_{pw}\frac{\partial T_w}{\partial t} = q_w D_i - q_c D_o \quad [8]$$

and

$$\rho_c c_{pc}\left(\frac{\partial T_c}{\partial t} + u_c\frac{\partial T_c}{\partial z}\right) = \frac{q_c D_o}{\frac{(D_2^2 - D_o^2)}{4}}. \quad [9]$$

Where D_o and D_i are, respectively, the outer and inner diameter of the condenser tube and D_2 is the inner diameter of the outer shell; T_w and T_c are the temperatures of the tube wall and coolant, respectively; q_w and q_c are the heat flux passing through the tube wall and that conveyed by the coolant, respectively; u_c is the average coolant velocity; ρ_w, c_{pw}, ρ_c and c_{pc} are the corresponding density and specific heat of tube wall and coolant.

2.2. Constitutive Equations

The following additional constitutive equations are required for closure of the system of equations.

2.2.1. Wall shear stress

The wall shear stress, τ_w, is defined as

$$\tau_w = -\frac{D_i}{4}\left(\frac{dp_F}{dz}\right), \quad [10]$$

where dp_F/dz is the frictional pressure gradient of the two-phase flow which can be evaluated using a Lockhart–Martinelli type correlation, i.e.

$$\left(\frac{dp_F}{dz}\right) = \Phi_G^2 \left(\frac{dp_F}{dz}\right)_G, \quad [11]$$

where

$$\Phi_G = \Phi_G(X_{tt}) \quad [12]$$

and

$$X_{tt} = \left[\frac{\left(\frac{dp_F}{dz}\right)_L}{\left(\frac{dp_F}{dz}\right)_G}\right]^{1/2}, \quad [13]$$

where

$$\left(\frac{dp_F}{dz}\right)_G \quad \text{and} \quad \left(\frac{dp_F}{dz}\right)_L$$

are given by

$$\left(\frac{dp_F}{dz}\right)_G = f_G \frac{4}{D_i} \frac{(Gx)^2}{2\rho_G} \quad [14]$$

and

$$\left(\frac{dp_F}{dz}\right)_L = f_L \frac{4}{D_i} \frac{[G(1-x)]^2}{2\rho_L}. \quad [15]$$

In these equations, G is the mass velocity of the two-phase flow and x denotes the flow quality, defined as

$$x = \frac{|\rho_G \epsilon u_G|}{|\rho_G \epsilon u_G| + |(1-\epsilon)\rho_L u_L|}; \quad [16]$$

the absolute sign in [16] is used in case of flow reversal. f_G And f_L are the friction factors for the gas or liquid phase alone flowing in the tube and can be computed from

$$f = \begin{cases} 0.079 \mathrm{Re}^{-0.25}, & 4000 < \mathrm{Re} < 30{,}000 \\ 0.046 \mathrm{Re}^{-0.2}, & 30{,}000 < \mathrm{Re}. \end{cases} \quad [17]$$

Equation [12], as presented by Soliman *et al.* (1968), takes the form

$$\Phi_G = 1 + 2.85 X_{tt}^{0.523} \quad [18]$$

2.2.2. Interfacial friction

The shear stress at the liquid–vapor interface is defined as

$$\tau_i = f_i \frac{\rho_G}{2} (u_G - u_L)^2, \quad [19]$$

where f_i is the interfacial friction factor. To account for the effect of interfacial roughness, a correlation proposed by Whalley & Hewitt (1978) is used:

$$f_i = f_G \left[1 + 24 \left(\frac{\rho_L}{\rho_G}\right)^{1/3} \frac{\delta}{D_i}\right], \quad [20]$$

where f_G is evaluated from [17] and δ is the thickness of the liquid film. In the annular flow model, [20] is written as

$$f_i = f_G \left[1 + 12 \left(\frac{\rho_L}{\rho_G}\right)^{1/3} (1 - \sqrt{\epsilon})\right]. \quad [21]$$

2.2.3. Condensation heat transfer coefficient

The heat transfer through the tube wall is given by

$$q_w = h_w(T_s - T_w). \quad [22]$$

Here T_s is the saturation temperature. The condensation heat transfer coefficient, h_w, is evaluated from the correlation of Azer *et al.* (1971), i.e.

$$h_w = 0.039 \mathrm{Re}_G^{0.9} \mathrm{Pr}_L^{0.337} \left(\frac{x^{0.9}}{4.67 - x}\right)\left(\frac{\eta_L}{\eta_G}\right)\left(\frac{\rho_G}{\rho_L}\right)^{0.5}\left(1.0 + 1.0986 X_{tt}^{0.039}\right)\frac{k}{D_i}. \quad [23]$$

Where Re_G is the gas phase Reynolds number and Pr_L is the liquid Prandtl number; η_G and η_L are the gas and liquid viscosities, respectively, and k is the thermal conductivity of the liquid phase.

2.2.4. Condensation rate

Since both the liquid and vapor phases are assumed to be at the saturation condition the condensation rate $\dot{\Gamma}$ is calculated from a simple energy jump relation:

$$\dot{\Gamma} = \frac{4}{D_i}\frac{q_w}{i_{GL}}, \quad [24]$$

where i_{GL} is the specific latent heat.

2.2.5. Physical properties

The physical properties of the condensing flow, such as densities, viscosities of the two phases, specific enthalpy and others are evaluated at their corresponding saturation pressure. The relationships of the physical properties to the pressure are constructed from the *ASHRAE Handbook—1985 Fundamentals Volume* (ASHRAE 1985) and the JSME Data Book (1983) *Thermophysical Properties of Fluid*, using the least-square fit method.

2.2.6. Heat transfer of coolant flow

The heat transferred to the coolant flow is given by

$$q_c = h_c(T_w - T_c). \quad [25]$$

The heat transfer coefficient of the coolant side, h_c, is evaluated from Kays & Leung's (1963) model for fully-developed turbulent flow in annuli. Their results were presented in tabulated form; thus, a least-square method is used to abstract the required values.

2.3. Boundary Conditions

At the condenser inlet, the refrigerant flow is 100% vapor at the saturation condition. The pressure and mass flowrate of the refrigerant are specified at the inlet, while the coolant temperature is given at the condenser outlet (coolant inlet). Three cases of flow transients are studied: (1) change in inlet pressure; (2) change in refrigerant inlet flowrate; and (3) change in coolant flowrate. To simulate the experimental conditions, changes in inlet pressure and the like between the initial and final states are prescribed by clamped cubic spline interpolations. The cubic spline interpolations yield continuous zeroth- to second-order derivatives.

3. SOLUTION METHOD

To solve the transient two-phase flow problem, a semi-implicit finite-difference numerical method is constructed. The spatial mesh used for the finite-difference equations is staggered, as shown in figure 2. Density, void fraction and other state variables are defined at the cell center; while velocities and pressure are defined at the cell edge. Values at other than defined locations are evaluated by linear interpolations. The divergence terms in the mass equations and the convective terms in the momentum equations involve donor-cell differences such that

$$\left(\frac{\partial Wu}{\partial z}\right)_j = \frac{\langle Wu\rangle_{j+\frac{1}{2}} - \langle Wu\rangle_{j+\frac{1}{2}}}{\Delta z_j}, \quad [26]$$

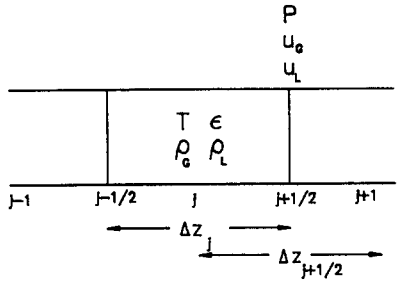

Figure 2. Computational mesh layout.

where

$$\langle Wu\rangle_{j+\frac{1}{2}}=\begin{cases}W_j u_{j+\frac{1}{2}} & \text{for } u_{j+\frac{1}{2}}\geqslant 0\\ W_{j+1}u_{j+\frac{1}{2}} & \text{for } u_{j+\frac{1}{2}}\leqslant 0\end{cases}, \qquad [27]$$

W can be any cell state variable or combination of such variables, u can be u_L or u_G and

$$\left(u\frac{\partial u}{\partial z}\right)_{j+\frac{1}{2}}=\begin{cases}\dfrac{u_{j+\frac{1}{2}}(u_{j+\frac{1}{2}}-u_{j-\frac{1}{2}})}{\Delta z_j}, & u_{j+\frac{1}{2}}\geqslant 0\\ \dfrac{u_{j+\frac{1}{2}}(u_{j+\frac{3}{2}}-u_{j+\frac{1}{2}})}{\Delta z_j}, & u_{j+\frac{1}{2}}\leqslant 0\end{cases}. \qquad [28]$$

With these notations, the resulting difference equations are given in the following. In the equations, superscripts n and $n+1$ refer to old- and new-time levels. An overbar above a quantity denotes that it is obtained as a 50% average between values at adjacent cells. To minimize subscripts, the cell indices j, except those specifying the cell edges, are omitted:

vapor mass equation,

$$\frac{\rho_G^{n+1}\epsilon^{n+1}-\rho_G^n\epsilon^n}{\Delta t}+\frac{\langle(\epsilon\rho_G)^n u_G^{n+1}\rangle_{j+\frac{1}{2}}-\langle(\epsilon\rho_G)^n u_G^{n+1}\rangle_{j+\frac{1}{2}}}{\Delta z}=-\dot{\Gamma}^{n+1}; \qquad [29]$$

liquid mass equation,

$$\frac{\rho_L^{n+1}(1-\epsilon)^{n+1}-\rho_L^n(1-\epsilon)^n}{\Delta t}+\frac{\langle[(1-\epsilon)\rho_L]^n u_L^{n+1}\rangle_{j+\frac{1}{2}}-\langle[(1-\epsilon)\rho_L]^n u_L^{n+1}\rangle_{j-\frac{1}{2}}}{\Delta z}=\dot{\Gamma}^{n+1}; \qquad [30]$$

momentum equation (1),

$$\begin{aligned}&(\epsilon\rho_G)^n_{j+\frac{1}{2}}\left[\left(\frac{u_G^{n+1}-u_G^n}{\Delta t}\right)\right]_{j+\frac{1}{2}}+(\epsilon\rho_G)^n_{j+\frac{1}{2}}\left(u_G\frac{\partial u_G}{\partial z}\right)^n_{j+\frac{1}{2}}\\&\quad+[(1-\epsilon)\rho_L]^n_{j+\frac{1}{2}}\left[\frac{u_L^{n+1}-u_L^n}{\Delta t}\right]_{j+\frac{1}{2}}+[(1-\epsilon)\rho_L]^n_{j+\frac{1}{2}}\left(u_L\frac{\partial u_L}{\partial z}\right)^n_{j+\frac{1}{2}}\\&=-\frac{p^{n+1}_{j+1}-p^{n+1}_j}{\Delta z_{j+\frac{1}{2}}}+\dot{\Gamma}^{n+1}_{j+\frac{1}{2}}(u_G^{n+1}-u_L^{n+1})_{j+\frac{1}{2}}-[\rho_G^{n+1}\epsilon^{n+1}+\rho_L^{n+1}(1-\epsilon^{n+1})]\boldsymbol{g}\cdot\sin\theta\\&\quad-\left\{\left(\frac{2}{D_i}f_i^n\sqrt{\epsilon^n}\rho_G^n\right)(u_G^{n+1}-u_L^{n+1})|u_G^n-u_L^n|\right\}_{j+\frac{1}{2}};\end{aligned} \qquad [31]$$

momentum equation (2),

$$\begin{aligned}&\epsilon^n[(1-\epsilon)\rho_G+\rho_L C_v]^n\left[\left(\frac{u_G^{n+1}-u_G^n}{\Delta t}\right)\right]_{j+\frac{1}{2}}-\epsilon^n[(1-\epsilon)\rho_L+\rho_L C_v]^n\left[\frac{u_L^{n+1}-u_L^n}{\Delta t}\right]_{j+\frac{1}{2}}\\&\quad+\{[\epsilon(1-\epsilon)\rho_G+\epsilon\rho_L C_v(\lambda-1)]u_G-\epsilon\rho_L C_v(\lambda-2)u_L\}^n\left(\frac{\partial u_G}{\partial z}\right)^n_{j+\frac{1}{2}}\\&\quad-\{[\epsilon(1-\epsilon)\rho_L+\epsilon\rho_L C_v(1-\lambda)]u_L+\epsilon\rho_L C_v\lambda u_G\}^n\left(\frac{\partial u_L}{\partial z}\right)^n_{j+\frac{1}{2}}\\&=\dot{\Gamma}^{n+1}(1-\epsilon^n)(u_G^{n+1}-u_L^n)+\epsilon^n(1-\epsilon^n)(\rho_L^{n+1}-\rho_G^{n+1})\boldsymbol{g}\cdot\sin\theta\\&\quad\times\left\{\left(\frac{2}{D_i}f_i^n\sqrt{\epsilon^n}\rho_G^n\right)(u_G^{n+1}-u_L^{n+1})|u_G^n-u_L^n|\right\}_{j+\frac{1}{2}}-\epsilon^n\left[\frac{4}{D_i}f_G^n\Phi_G^2G^{n+1}|G|^n\right]_{j+\frac{1}{2}};\end{aligned} \qquad [32]$$

wall conduction equation,

$$\rho_w c_{pw} \frac{(D_o^2 - D_i^2)}{4} \frac{(T_w^{n+1} - T_w^n)}{\Delta t} = h_w^{n+1} D_i (T_s^{n+1} - T_w^{n+1}) - h_c^{n+1} D_o (T_w^{n+1} - T_c^{n+1}); \quad [33]$$

and

coolant energy equation,

$$\rho_c c_{pc} \left(\frac{T_c^{n+1} - T_c^n}{\Delta t} + u_c^{n+1} \frac{T_{c,j}^{n+1} - T_{c,j-1}^{n+1}}{\Delta z_j} \right) = \frac{h_c^{n+1} (T_w^{n+1} - T_c^{n+1}) D_o}{\frac{(D_2^2 - D_o^2)}{4}}. \quad [34]$$

It is noted that the semi-implicit numerical scheme treats the mass and momentum equations with mixed implicitness, while the wall condition and coolant energy equations are completely implicit. Numerical analysis and experience have shown that this scheme is numerically stable provided that the time steps are within the convective Courant criterion, i.e.

$$\Delta t \leqslant \max \left\{ \frac{\Delta z_j}{u_G}, \frac{\Delta z_j}{u_L} \right\}. \quad [35]$$

To proceed with the numerical calculation, the new-time velocities in the mass equations are eliminated by using the momentum equations in favor of the new-time pressures, resulting in a void–pressure system of equations. At each time step, the pressure–void equations and the coolant energy and wall conduction equations, together with constitutive relations, are solved iteratively using the Newton–Raphson method. In the calculation, the coefficient of the virtual mass force, C_v, is set equal to 0.03 and $\lambda = 1$. Numerical tests indicate that the inclusion of the virtual mass force does improve the numerical efficiency considerably and choices of C_v from 0.01 to 0.05 and λ from 0 to 2 do not appreciably affect the numerical results.

For a typical 10 s flow transient in a condenser divided into 30 mesh cells, the computation time with a time step of 0.07 s is about 20 min on an IBM PC/AT. As can be seen from [35], the time step is restricted by the mesh size. If the number of mesh cells is increased to 40, the computation time would be increased by a factor of 2; but the calculated results would not be affected significantly. Thus, generally, a mesh number of 30 is used in the present calculation.

4. NUMERICAL RESULTS AND DISCUSSION

Numerical calculations were performed for a test condenser consisting of a 7.75 mm i.d. × 9.75 mm o.d. × 5.24 m long copper tube located concentrically within a 19.2 mm i.d. water jacket. The refrigerant is freon-22. Attention is focused upon the responses of the void fraction and outlet condensate flowrate during the transient.

Figure 3 shows the responses of the outlet flowrate to a decrease in inlet pressure from 1.3 to 1.1 MPa, with the other conditions kept constant. The periods of the pressure transients are 2, 5 and 8 s, respectively, as indicated in the figure. In this and the following figures, $\dot{m}_{out}$ and $\dot{m}_{in}$ denote

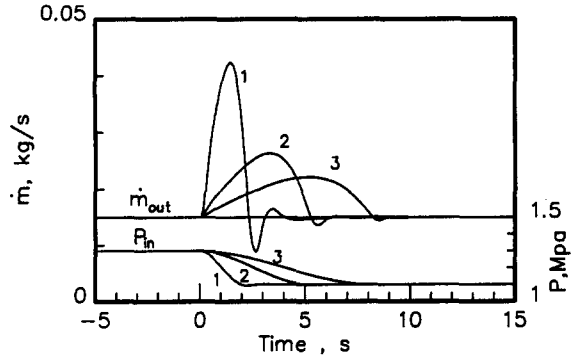

Figure 3. Response of the outlet condensate flowrate after decreasing the inlet pressure.

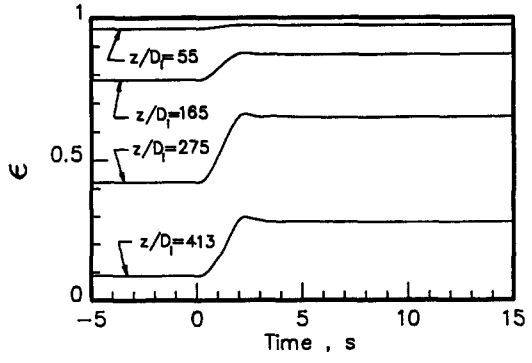

Figure 4. Void fraction response to a decrease in inlet pressure.

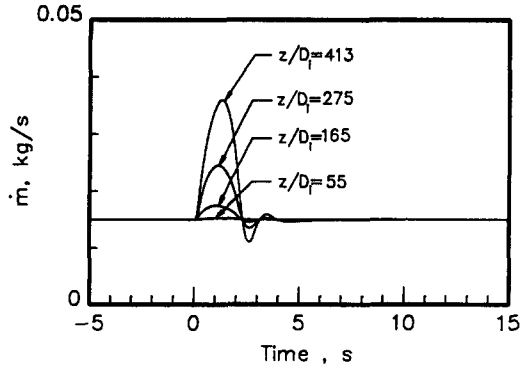

Figure 5. Mass flowrate response to a decrease in inlet pressure.

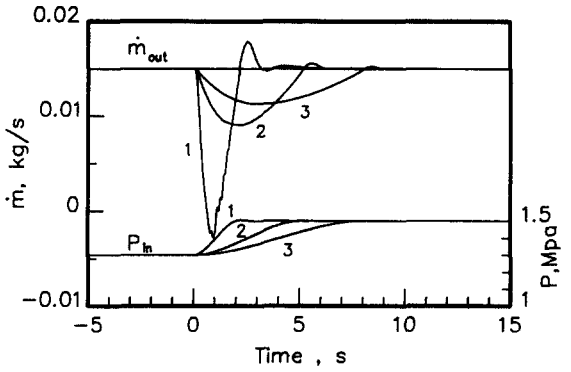

Figure 6. Response of the outlet condensate flowrate after increasing the inlet pressure.

the outlet and inlet refrigerant mass flowrates, $\dot{m}_c$ is the coolant mass flowrate and p_{in} is the inlet pressure. Figure 3 shows that the outlet mass flowrate increases dramatically after the pressure begins to change, followed by a decay back to the initial flowrate. The flow surge phenomenon is more pronounced as the transient period is decreased. This phenomenon is caused by an increase in the vapor void fraction in the condenser. Void fraction responses at four locations for the case of the 2 s pressure transient are illustrated in figure 4. One can see that the void fractions at all the locations increase as a result of the pressure decrease. The total void of the two-phase flow is subsequently increased, which displaces the liquid and causes the outlet flowrate to be momentarily larger than the inlet flowrate. In fact, for this transient, the point of complete condensation has moved from $z/D_i = 573$ to a final value of 625. Figure 5 shows the variation of mass flowrate at four positions for the same transient; the transient surge is more visible closer to the downstream. An oscillatory flow behavior at the end of the transient is noticed. This is a result of the clamped cubic spline formulation of the pressure variation. As revealed in figure 3, the oscillatory behavior at the end of the pressure transient is hardly noticeable; however, it causes the flow to respond vigorously. This result may explain the fluctuating nature of the two-phase flow in which a pressure perturbation is easily encountered.

Figure 6 shows the outlet flow responses when the inlet pressure is increased from 1.3 to 1.5 MPa. The pressure transient periods are also 2, 5 and 8 s, respectively. As the pressure is increased, the vapor is compressed. In the mean time the condensation heat transfer rate is increased due to the rise in vapor density and saturation temperature. These factors jointly reduce the vapor void fraction of the condensing flow, resulting in a momentary decrease in the condensate flow. If the transient occurs very rapidly as in the case of the 2 s pressure transient, a flow reversal occurs for a short period. At the time when the rate of change of the void fraction starts to slow down (point of inflexion), the outlet condensate flow begins to revert to the initial flowrate. For this case, the point of complete condensation has moved from $z/D_i = 573$ to 512.

If the inlet pressure is kept constant while the inlet vapor is increased by 40% from 0.015 to 0.021 kg/s (corresponding to an increase in Re from 210,000 to 294,000) in 2, 5 and 8 s, the responses of the outlet flow are as shown in figure 7. Physically, similar mechanisms in the case of changes in inlet pressure are present in this situation. The initial increase in the outlet flow is a result of the displacement of liquid by vapor. The point of complete condensation for this case has moved from $z/D_i = 573$ to a final value of 584. The movement is much smaller than in the previous case. The maximum outlet flowrate encountered during the 2 s inlet flow transient is 0.029 kg/s. As a comparison, it is 0.042 kg/s, as shown in figure 3, for an 18% decrease in the inlet pressure in 2 s. Figure 8 shows the responses of the outlet flowrate as the inlet vapor flow is decreased by 40%. Flow reversal occurs when the inlet flowrate is decreased in 2 s. Flow oscillation, though not easily observed, is also noted.

For the case where the inlet pressure and flowrate of the condensing flow are held constant but the coolant flowrate is subjected to either a decrease or an increase of 50%, the transient responses of the outlet condensate flow are as shown in figures 9 and 10, respectively. It is seen that the responses are slower than those relating to changes in inlet pressure or inlet vapor flow. Changing

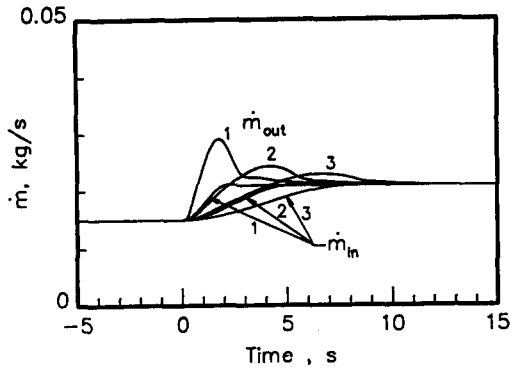

Figure 7. Response of the outlet condensate flowrate after increasing the inlet mass flowrate.

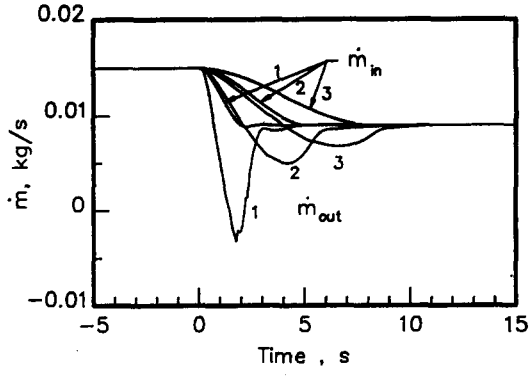

Figure 8. Response of the outlet condensate flowrate after decreasing the inlet mass flowrate.

the coolant flowrate causes the tube wall temperature, and subsequently the condensation rate, to change. The thermal capacity of the tube wall acts to slow down the response. The resistance to convective heat transfer in the coolant side as well as to condensation heat transfer also plays a role in slowing down the response. The response in a situation of decreasing coolant flow is thus even slower. One can see from figure 9 that the condensate flows have not reached the final steady state after 15 s, even for the shortest coolant transient. Unlike previous cases, no flow reversal or oscillation are found in figures 9 and 10.

5. EXPERIMENTAL OBSERVATIONS

5.1. Description of Apparatus

A schematic of the experimental apparatus is shown in figure 11. It is a conventional refrigeration cycle consisting primarily of a compressor, an oil separator, a pre-condenser, a condenser test section, an expansion valve and an evaporator. The working fluid is freon-22. The loop piping connecting each element is made of 3/8″ copper tube (9.75 mm o.d. × 1.0 mm thick).

The superheated R-22 vapor is generated from the evaporator before it is compressed to the desired system pressure by the compressor. The evaporator is of tube-and-shell type. The compressor, which is 1.0 ton in capacity, is driven by a 60 Hz a.c. motor. A motor controller, or inverter, is provided to regulate the frequency of the motor.

Leaving the compressor, the vapor refrigerant passes in series through the oil separator and pre-condenser and into the test section. The oil separator removes the oil moisture pumped from the compressor. The pre-condenser is used to remove any superheat from the vapor before it enters the test section. The horizontally settled condenser test section, having a total length of 5.24 m, is a concentric tube configuration. The inner tube is of the same size as the looping system, while the outer tube is made of SS304 with 19.2 mm i.d. The refrigerant vapor condenses inside the inner

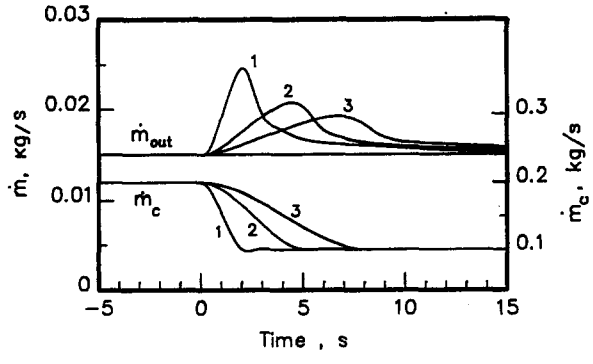

Figure 9. Response of the outlet condensate flowrate after decreasing the coolant mass flowrate.

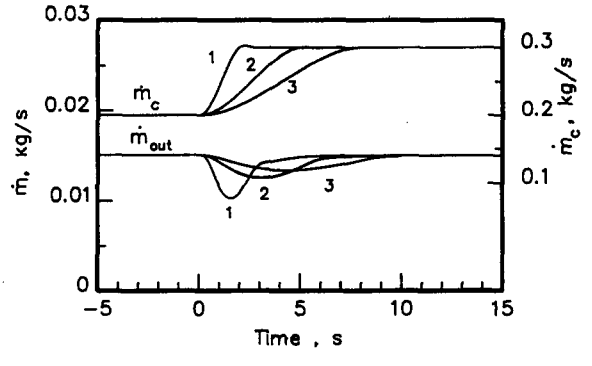

Figure 10. Response of the outlet condensate flowrate after increasing the coolant mass flowrate.

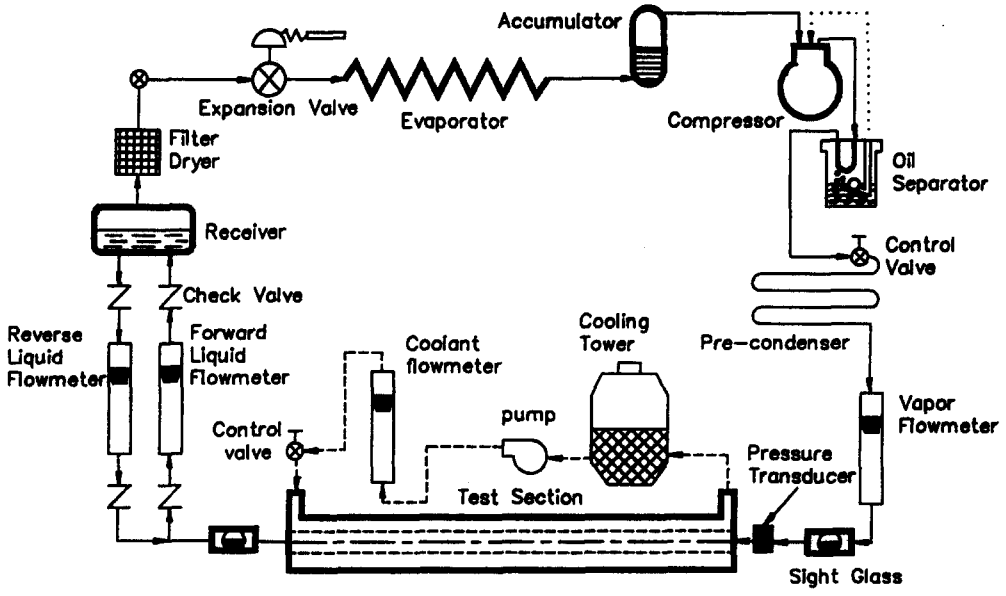

Figure 11. Schematic of the experimental apparatus.

tube and the water coolant flows countercurrently in the annulus. The coolant loop consists of a pump, a cooling tower and a flowmeter. In addition, two sight glass (Pyrex glass) having the same inner diameter as the condenser tube are installed, respectively, ahead of and behind the condenser for observing the flow condition. Two control valves, one located at the compressor outlet and the other at the coolant inlet, are provided for, respectively, regulating the refrigerant inlet flowrate and the coolant flowrate.

Leaving the condenser test section, the liquid flows through an outlet flowrate measuring section which consists of a pair of rotameters and four quick-acting check valves. Forward flow is measured by one of the flowmeters and the reversed flow, should it occur, is measured by the other. The four check valves ensure unidirectional flow through either of the two flowmeters. Departing from the measuring section, the freon-22 passes through the expansion value and enters the evaporator to complete the cycle.

5.2. Instrumentation

A pressure transducer is installed at the inlet of the condenser tube to measure the static pressure of the vapor inlet flow. The transducer, which is of strain-gauge type with $\pm 3\%$ uncertainty, has a range of 0–3.0 MPa. The flowrates of the vapor refrigerant, liquid condensate and coolant flows are measured with rotameter-type flowmeters. During the transient, the displacement of the rotameter float is sensed magnetically and transformed into 0–2 V electrical output signals. The errors associated with the vapor and condensate refrigerant flowrates are estimated to be within $\pm 6.5\%$, while that associated with the coolant flowrate is $\pm 2.5\%$.

Four thermocouples (K type) are installed to measure the temperatures of the refrigerant and coolant flows, respectively, at the inlet and exit of the test section. The temperature measurements are primarily for calibration purpose and for checking the flow condition during the tests.

All the signals, including those from thermocouples, flowmeters and pressure transducer, are collected by a data acquisition system which contains an IBM PC/AT, an A/D converter and an EXP-16 multiplexer-amplifier. Signals from the thermocouples are first amplified in the multiplexer-amplifier and converted by the A/D converter, while signals from the pressure transducer and flowmeters are converted directly. All the converted digital signals are sent to the host computer for further operations.

5.3. Comparison of Experimental Data with Numerical Results

For a typical transient run, the steady flow condition was established. Then, a change in the refrigerant inlet flowrate or the coolant flowrate was initiated by manually turning one of the

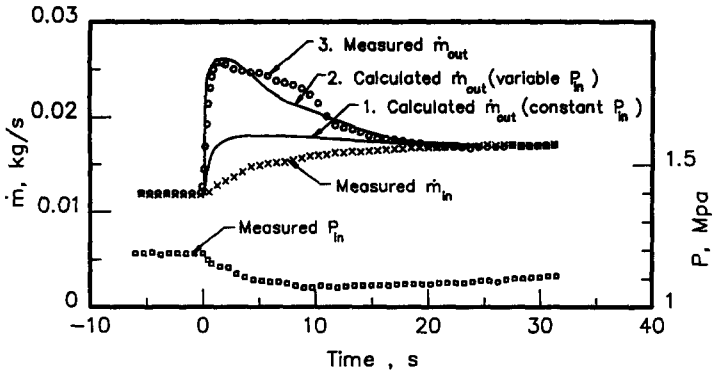

Figure 12. Comparison of experimental data with calculations for an increase in inlet flowrate.

control valves, to trigger the transient process. The measured responses of the outlet condensate flow and the inlet pressure, for a test run of increasing the inlet flowrate from 0.0118 to 0.0171 kg/s, are given in figure 12. The variation of the inlet flowrate is also displayed in the figure. The outlet condensate flow exhibits flow surge characteristics and it is noted that, during the transient, the condensing pressure was changing.

For the purpose of comparison, the response of the outlet flow due to the change in inlet flowrate alone was calculated and the result is shown by curve 1 in figure 12. In the calculation, the variation of the inlet flowrate was represented by clamped cubic spline interpolations of 8 data points. It is seen that the calculation under the assumption of constant inlet pressure considerably underpredicts the measured data. However, when the variation of the inlet pressure together with the change in the inlet flowrate was introduced, the calculated result, shown by curve 2, agrees with the data excellently.

For the case where the coolant flowrate was increased from 0.105 to 0.235 kg/s (a 124% increase!) in 2 s, the measured responses of the inlet pressure and the refrigerant inlet and outlet flowrates are plotted in figure 13. The figure shows that the inlet pressure decreased gradually to a new steady-state value and the inlet flowrate first increased and thereupon decayed to another steady-state value (specifically, a 2.8% increase in the initial flowrate). The interesting aspect of this transient is the oscillatory response of the condensate outlet flowrate.

As discussed in the theoretical analysis, for an increase in coolant flowrate, the outlet condensate flow would decrease as a result of the decreasing vapor void inside the condenser. A substantial decrease, even a flow reversal, would be expected to occur for such a large increase in the coolant flowrate in such a short time. However, both increasing the inlet flowrate and decreasing the condensing pressure, as observed in this test, would result in increasing the outlet flowrate and, in turn, offsetting and distorting the effect of changing the coolant flowrate alone. Imposing those factors on the theoretical calculation, one obtains the response of the outlet flowrate, as shown by the solid curve in figure 13. Though the calculated result does not exactly follow the experimental data, it does reveal the oscillatory characteristics of the outlet condensate flow. The difference

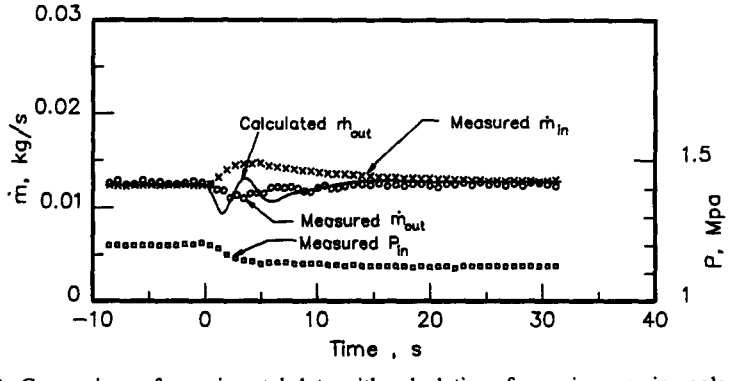

Figure 13. Comparison of experimental data with calculations for an increase in coolant flowrate.

between the calculated and the measured results can be attributed to the facts that the response is very sensitive to the time rate of change of pressure and a slight deviation in input of that information may cause the theoretical result to differ considerably.

Figures 12 and 13 illustrate the transient phenomena of a condensing flow can be predicted very well with the present model as long as all the effects induced by the input change have been included in the analysis.

6. CONCLUSIONS

The conclusions drawn from this investigation, of the transient response of the condensing flow in a horizontal double-pipe condenser due to system input changes, are summarized as follows:

(1) The two-phase two-fluid model, together with the constitutive relations, is capable and adequate to analyze and interpret the experimental data of the dynamic behavior of a condensing system. Inclusion of the virtual mass force in the momentum equation has considerably improved the numerical stability and efficiency. The choice of the coefficients of the virtual mass force within a certain range does not appreciably affect the numerical results.

(2) A change in system input (inlet vapor flowrate, inlet pressure or coolant flowrate) causes the vapor void in the condenser to change, which gives rise to the flow surge phenomenon in the outlet condensate flow. The response of the condensing flow is very sensitive to the change in inlet pressure. The response to change in the coolant side is rather slow, due to the thermal capacity of the tube wall which slows down the response.

(3) The experimental data indicate that the condensing pressure has not remained constant during the transient of changing the inlet flowrate or coolant flowrate. The flow surge in the condensate flow, for the case of changing the inlet flowrate, is enlarged as a result of the pressure variation. For the case of a change in coolant flowrate, the experimental data reveals the oscillatory characteristics of the outlet condensate flow. The measured transient phenomena are well-predicted and interpreted by the present analysis.

Acknowledgement—This work was supported by the National Science Council, Taiwan, R.O.C., under Grant Nos NSC76-0401-E009-02 and -06.

REFERENCES

ASHRAE 1985 *ASHRAE Handbook—1985 Fundamentals Volume.* ASHRAE, Atlanta, Ga.

AZER, N. Z., ABIS, L. V. & SWEARINGEN, T. B. 1971 Local heat transfer coefficients during forced convection condensation inside horizontal tubes. *ASHRAE Trans.* **77** (Part 1), 182–201.

DREW, D. A., CHENG, L. Y. & LAHEY, R. T. JR 1979 The analysis of virtual mass effects in two-phase flow. *Int. J. Multiphase Flow* **5,** 233–242.

JSME DATA BOOK 1983 *Thermophysical Properties of Fluids.* JSME, Tokyo.

KAYS, W. M. & LEUNG, E. Y. 1963 Heat transfer in annular passages—hydrodynamically developed turbulent flow with arbitrarily prescribed heat flux. *Int. J. Heat Mass Transfer* **6,** 537–557.

LAHEY, R. T. JR, CHENG, L. Y., DREW, D. A. & FLAHERTY, J. E. 1980 The effect of virtual mass on the numerical stability of accelerating two-phase flows. *Int. J. Multiphase Flow* **6,** 281–294.

LIAO, N. S., WANG, C. C. & TIEN, C. L. 1988 Analysis of flow surge phenomena in a single-tube condenser. *Int. Commun. Heat Mass Transfer* **15,** 257–268.

MCMORRAN, P. O. & MOECK, E. O. 1976 Dynamic model of condensation in a tube. Report AECL-5603.

NO, C. H. & KAZIMI, M. S. 1985 Effects of virtual mass on the mathematical characteristics and numerical stability of the two-fluid model. *Nucl. Sci. Engng* **89,** 197–206.

SCHOENBERG, A. A. 1966 Mathematical model with experimental verification for the dynamic behavior of a single-tube condenser. Report NASA TN D-3453.

SOLIMAN, M., SCHUSTER, J. R. & BERENSON, P. J. 1968 A general heat transfer correlation for annular flow condensation. *Trans. ASME Ser. C., J. Heat Transfer* **90,** 267–276.

WEDEKIND, G. L. & BHATT, B. L. 1977 An experimental and theoretical investigation into thermally governed transient flow in two-phase condensing flow. *J. Heat Transfer* **99,** 561–567.

WHALLEY, P. B. & HEWITT, G. F. 1977 The correlation of liquid entrainment fraction and entrainment rate in annular two phase flow. Report AERE-R9187.

YADIGAROGLU, G. & LAHEY, R. T. JR 1976 On the various forms of the conservation equations in two-phase flow. *Int. J. Multiphase Flow* **2,** 477–494.

ZUBER, N. & STAUB, F. W. 1966 The propagation and wave form of the vapor volumetric concentration. *Int. J. Heat Mass Transfer* **9,** 871–895.